

TURBO CODED OFDM-OQAM USING HILBERT TRANSFORM

Kasturi Vasudevan¹, Surendra Kota¹, Lov Kumar¹,
Himanshu Bhusan Mishra²

¹Dept of EE IIT Kanpur India;

²Dept of Electronics IIT-ISM Dhanbad India

Keywords: OFDM-OQAM, FBMC, GFDM, OFDM, SSB, frequency offset, average SNR per bit, BER, matched filter, Hilbert transform, turbo code.

ABSTRACT

Orthogonal frequency division multiplexing (OFDM) with offset quadrature amplitude modulation (OQAM) has been widely discussed in the literature and is considered a popular waveform for 5th generation (5G) wireless telecommunications and beyond. In this work, we show that OFDM-OQAM can be generated using the Hilbert transform and is equivalent to single sideband modulation (SSB), that has roots in analog telecommunications. The transmit filter for OFDM-OQAM is complex valued whose real part is given by the pulse corresponding to the root raised cosine spectrum and the imaginary part is the Hilbert transform of the real part. The real-valued digital information (message) are passed through the transmit filter and frequency division multiplexed on orthogonal subcarriers. The message bandwidth corresponding to each subcarrier is assumed to be narrow enough so that the channel can be considered ideal. Therefore, at the receiver, a matched filter can be used to recover the message. Turbo coding is used to achieve bit-error-rate (BER) as low as 10^{-5} at an average signal-to-noise ratio (SNR) per bit close to 0 db. The system has been simulated in discrete time.

INTRODUCTION

Orthogonal frequency division multiplexing (OFDM) [1-3] and OFDM offset quadrature amplitude modulation (OFDM-OQAM) [4] are the preferred modulation techniques for transmission of digital information over frequency selective channels, both fading and non-fading. The variants of OFDM-OQAM [5-9] are known as filter bank multicarrier (FBMC) [4-7] and universal filtered multicarrier (UFMC) [10, 11] and generalized frequency division multiplexing (GFDM) [12-14] in the literature.

One of the key advantages of OFDM-OQAM/FBMC/UFMC over OFDM is its immunity against carrier frequency offsets (CFO). In other words, it may not be necessary for an OFDM-OQAM/FBMC/UFMC system to estimate and cancel the CFO, unlike OFDM. However, it has been shown in [1-3] that it is possible to estimate and cancel the CFO very accurately with large scope for parallel processing. The other important feature of OFDM-OQAM is the spectral containment of each subcarrier using a transmit filter, which

is absent in OFDM. However, OFDM is more attractive than OFDM-OQAM in terms of implementation simplicity.

In this work, we demonstrate that OFDM-OQAM/FBMC/UFMC can be efficiently implemented using the Hilbert transform at the transmitter and a matched filter at the receiver [15]. It must be noted that using OQAM would improve the symbol density in time-frequency space, at the cost of introducing intersymbol interference (ISI) at the matched filter output and increasing the receiver complexity. Therefore, in this work, we do not use OQAM and yet have a symbol density in time frequency space greater than unity. We however retain the nomenclature ‘‘OFDM-OQAM/FBMC/UFMC’’ since this work deals with multicarrier communications.

We use the following notation. Complex quantities are denoted by a tilde e.g., $\tilde{p}(t)$, estimates are denoted by hat e.g., \hat{b} and convolution is denoted by star e.g., $p(t) \star g(t)$. This article is organized as follows. We first discuss the theory of OFDM-OQAM, followed by derivation of Hilbert transform of the pulse corresponding to root-raised cosine spectrum. The discrete-time implementation issues are discussed next, motivating the need for a modified Hilbert transform. The discrete-time system model used for computer simulations is presented, followed by results and conclusions.

THEORY

At the outset, we note that multicarrier communication is equivalent to frequency division multiplexing. The time-frequency representation of a multicarrier communication system is shown in Figure 1 [4]. The symbol-rate is $1/T$ baud and the subcarrier spacing is \mathcal{B} . The red colour dots denote symbols. The subcarrier frequency can be positive or negative, as will be apparent later. The complex envelope of a linearly modulated digital signal is given

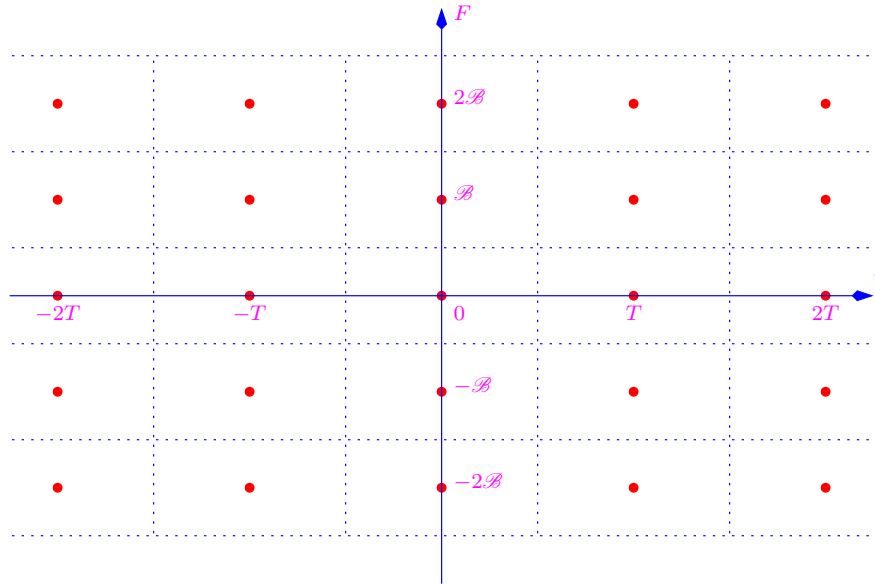


Figure 1: Symbol density of multicarrier communication system in time-frequency space.

by [16]

$$\begin{aligned}
 \tilde{s}(t) &= \sum_{k=-\infty}^{\infty} S_k \tilde{p}(t - kT) \\
 &= s_I(t) + j s_Q(t) \quad (\text{say})
 \end{aligned} \tag{1}$$

where S_k denotes complex-valued symbols drawn from an M -ary constellation, $\tilde{p}(t)$ denotes the (possibly complex-valued) impulse response of the transmit filter, the subscripts “ I, Q ” denote in-phase (real) and quadrature (imaginary) components respectively. When the symbols S_k are uncorrelated, the power spectral density of $\tilde{s}(t)$ in (1) is [16]

$$S_{\tilde{s}}(F) = \frac{P_{\text{av}}}{2T} \left| \tilde{P}(F) \right|^2 \quad (2)$$

where $\tilde{P}(F)$ is the Fourier transform of $\tilde{p}(t)$ and P_{av} denotes the average power of the M -ary constellation. If the transmit filter $\tilde{p}(t) = p(t)$ is real-valued [16] having a root raised cosine (RRC) spectrum with roll-off factor ρ , $0 < \rho \leq 1$, then the minimum spacing between subcarriers for no aliasing would be

$$\mathcal{B} = \frac{2(1 + \rho)}{2T} \quad (3)$$

which is essentially the two-sided bandwidth of $\tilde{P}(F)$. Therefore, the symbol density in time-frequency space is the inverse of the area of each rectangle in Figure 1 [4]:

$$\frac{1}{\mathcal{B}T} = \frac{1}{(1 + \rho)} < 1. \quad (4)$$

In this article, we propose a complex-valued transmit filter given by

$$\tilde{p}(t) = p(t) + j\hat{p}(t) \quad (5)$$

where $p(t)$ has an RRC spectrum and $\hat{p}(t)$ is the Hilbert transform of $p(t)$. The Fourier transform of $\tilde{p}(t)$ in (5) is

$$\begin{aligned} \tilde{P}(F) &= P(F) + j(-j\text{sgn}(F))P(F) \\ &= \begin{cases} 2P(F) & \text{for } F > 0 \\ P(0) & \text{for } F = 0 \\ 0 & \text{for } F < 0 \end{cases} \end{aligned} \quad (6)$$

where $P(F)$ is the Fourier transform of $p(t)$ and $\text{sgn}(\cdot)$ is the signum function [17, 18]. The minimum spacing between subcarriers in this case is

$$\mathcal{B} = \frac{1 + \rho}{2T} \quad (7)$$

resulting in symbol density in time-frequency space equal to

$$\frac{1}{\mathcal{B}T} = \frac{2}{(1 + \rho)} \geq 1. \quad (8)$$

It is emphasized here that when $\tilde{p}(t)$ is given by (5), the symbols S_k have to be real-valued. The reason is as follows. The complex envelope in (1) can be written as

$$\tilde{s}(t) = \tilde{s}_1(t) \star \tilde{p}(t) \quad (9)$$

where “ \star ” denotes convolution and

$$\tilde{s}_1(t) = \sum_{k=-\infty}^{\infty} S_k \delta_D(t - kT)$$

$$= s_{1,I}(t) + j s_{1,Q}(t) \quad (\text{say}) \quad (10)$$

where $\delta_D(\cdot)$ denotes the Dirac-delta function [17,18]. At the receiver, we use a matched filter given by $\tilde{p}^*(-t)$. The matched filter output would be given by [16]

$$\tilde{y}(t) = \tilde{s}_1(t) \star \tilde{p}(t) \star \tilde{p}^*(-t). \quad (11)$$

Now

$$\begin{aligned} \tilde{p}(t) \star \tilde{p}^*(-t) &= [p(t) + j\hat{p}(t)] \star [p(-t) - j\hat{p}(-t)] \\ &= p(t) \star p(-t) + \hat{p}(t) \star \hat{p}(-t) + j [\hat{p}(t) \star p(-t) - p(t) \star \hat{p}(-t)]. \end{aligned} \quad (12)$$

It can be shown that for real-valued $p(t)$ [17,18]

$$\begin{aligned} \hat{p}(t) \star \hat{p}(-t) &= p(t) \star p(-t) \\ &= R_{pp}(t) \\ \hat{p}(t) \star p(-t) &= R_{\hat{p}p}(t) \\ &= -p(t) \star \hat{p}(-t) \\ &= -R_{p\hat{p}}(t). \end{aligned} \quad (13)$$

Substituting (12) and (13) in (11) we obtain the matched filter output as

$$\tilde{y}(t) = \sum_{k=-\infty}^{\infty} 2S_k [R_{pp}(t - kT) + j R_{\hat{p}p}(t - kT)]. \quad (14)$$

The condition for zero ISI is

$$R_{pp}(mT) = \delta_K(mT) \quad (15)$$

where $\delta_K(\cdot)$ is the Kronecker delta function [16]. However, $R_{\hat{p}p}(t)$ does not satisfy the zero ISI condition. Hence using (15), the symbol-rate sampler at the matched filter output would yield

$$\begin{aligned} \tilde{y}(nT) &= \sum_{k=-\infty}^{\infty} 2S_k (R_{pp}(nT - kT) + j R_{\hat{p}p}(nT - kT)) \\ &= 2S_n + 2j \sum_{k=-\infty}^{\infty} S_k R_{\hat{p}p}(nT - kT). \end{aligned} \quad (16)$$

It is clear from (16) that implementing the matched filter as given in (11) and (12) with complex-valued symbols S_k is not possible, due to crosstalk (interference between in-phase and quadrature components). Therefore, the symbols S_k have to be real-valued. One possible implementation of the proposed OFDM-OQAM/FBMC/UFMC transmitter is shown in Figure 2. The corresponding receiver is shown in Figure 3. In the next section, we derive $\hat{p}(t)$ when $p(t)$ has an RRC spectrum.

HILBERT TRANSFORM OF RRC SPECTRUM

The RRC spectrum which is the Fourier transform of $p(t)$ is given by [16]

$$P(F) = \begin{cases} \frac{1}{\sqrt{2B}} & \text{for } -F_1 \leq F \leq F_1 \\ \frac{1}{\sqrt{2B}} \cos\left(\frac{\pi(|F|-F_1)}{4B-4F_1}\right) & \text{for } F_1 \leq |F| \leq 2B - F_1 \\ 0 & \text{elsewhere} \end{cases} \quad (17)$$

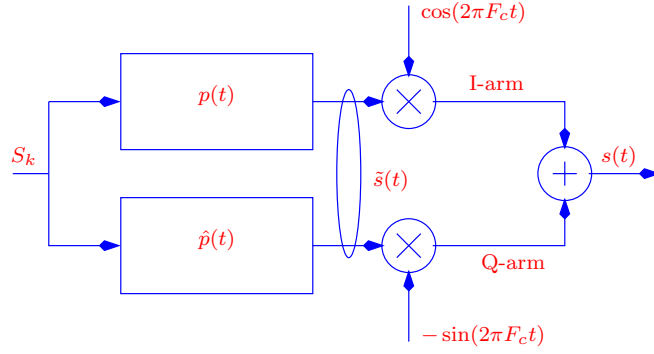


Figure 2: Proposed OFDM-OQAM transmitter for each subcarrier.

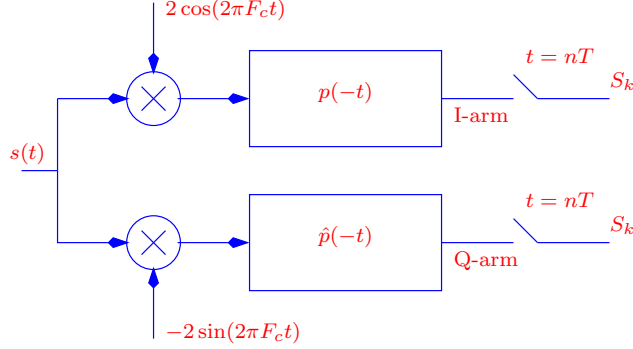


Figure 3: Proposed OFDM-OQAM receiver for each subcarrier.

where

$$2B \triangleq \frac{1}{T}$$

$$\rho \triangleq 1 - \frac{F_1}{B}. \quad (18)$$

Therefore

$$\hat{p}(t) = \int_{F=-\infty}^{\infty} -j \operatorname{sgn}(F) P(F) e^{j2\pi Ft} dF \quad (19)$$

where $P(F)$ is given by (17) and (18). We have

$$I_1 = \int_{F=-F_1}^{F_1} -j \operatorname{sgn}(F) \frac{1}{\sqrt{2B}} e^{j2\pi Ft} dF$$

$$= \frac{1}{\pi t \sqrt{2B}} [1 - \cos(2\pi F_1 t)]. \quad (20)$$

Similarly

$$I_2 = \int_{F=F_1}^{2B-F_1} -j \frac{1}{\sqrt{2B}} \cos\left(\frac{\pi(F-F_1)}{4B-4F_1}\right) e^{j2\pi Ft} dF$$

$$+ \int_{F=-(2B-F_1)}^{-F_1} j \frac{1}{\sqrt{2B}} \cos\left(\frac{\pi(-F-F_1)}{4B-4F_1}\right) e^{j2\pi Ft} dF$$

$$= \frac{1}{\sqrt{2B}} \int_{F=B(1-\rho)}^{B(1+\rho)} \left\{ \sin\left[2\pi Ft + \frac{\pi(F-F_1)}{4B-4F_1}\right] + \sin\left[2\pi Ft - \frac{\pi(F-F_1)}{4B-4F_1}\right] \right\} dF$$

$$\begin{aligned}
&= \frac{1}{\sqrt{2B}} \int_{F=B(1-\rho)}^{B(1+\rho)} \{\sin[\alpha F - \beta] + \sin[\beta - \gamma F]\} dF \\
&= \frac{1}{\gamma\sqrt{2B}} \{\cos[\beta - \gamma B(1 + \rho)] - \cos[\beta - \gamma B(1 - \rho)]\} \\
&\quad - \frac{1}{\alpha\sqrt{2B}} \{\cos[\alpha B(1 + \rho) - \beta] - \cos[\alpha B(1 - \rho) - \beta]\}
\end{aligned} \tag{21}$$

where

$$\begin{aligned}
F_1 &= B(1 - \rho) \\
2B - F_1 &= B(1 + \rho) \\
4B - 4F_1 &= 4B\rho \\
\alpha &= \frac{\pi(1 + 8Bt\rho)}{4B\rho} \\
\beta &= \frac{\pi F_1}{4B\rho} \\
\gamma &= \frac{\pi(1 - 8Bt\rho)}{4B\rho}.
\end{aligned} \tag{22}$$

Now from (22)

$$\begin{aligned}
\beta - \gamma B &= \frac{-\pi}{4} + 2\pi Bt \\
\gamma B\rho &= \frac{\pi}{4} - 2\pi Bt\rho \\
\alpha B - \beta &= \frac{\pi}{4} + 2\pi Bt \\
\alpha B\rho &= \frac{\pi}{4} + 2\pi Bt\rho.
\end{aligned} \tag{23}$$

Substituting (23) in (21) we obtain

$$\begin{aligned}
I_2 &= \frac{1}{\sqrt{2B}} \sin(2\pi Bt(1 + \rho)) \left\{ \frac{1}{\gamma} + \frac{1}{\alpha} \right\} \\
&\quad - \frac{1}{\sqrt{2B}} \cos(2\pi Bt(1 - \rho)) \left\{ \frac{1}{\gamma} - \frac{1}{\alpha} \right\}.
\end{aligned} \tag{24}$$

Now

$$\begin{aligned}
\frac{1}{\gamma} - \frac{1}{\alpha} &= \frac{64B^2\rho^2t}{\pi(1 - 64B^2t^2\rho^2)} \\
\frac{1}{\gamma} + \frac{1}{\alpha} &= \frac{8B\rho}{\pi(1 - 64B^2t^2\rho^2)}.
\end{aligned} \tag{25}$$

Substituting (25) in (24) we get

$$\begin{aligned}
I_2 &= \frac{1}{\sqrt{2B}} \sin(2\pi Bt(1 + \rho)) \left\{ \frac{8B\rho}{\pi(1 - 64B^2t^2\rho^2)} \right\} \\
&\quad - \frac{1}{\sqrt{2B}} \cos(2\pi Bt(1 - \rho)) \left\{ \frac{64B^2\rho^2t}{\pi(1 - 64B^2t^2\rho^2)} \right\}.
\end{aligned} \tag{26}$$

Finally $\hat{p}(t)$ in (19) is given by

$$\hat{p}(t) = I_1 + I_2 \tag{27}$$

where I_1 , I_2 are given by (20) and (26) respectively.

DISCRETE TIME IMPLEMENTATION

Theoretically when $p(t)$ has an RRC spectrum, both $p(t)$, $\hat{p}(t)$ have an infinite time span. In practice they have to be truncated, in which case (15) is only approximately valid. Moreover, the transmitter and receiver in Figures 2 and 3 have to be implemented in discrete time. In this section, we explore these issues.

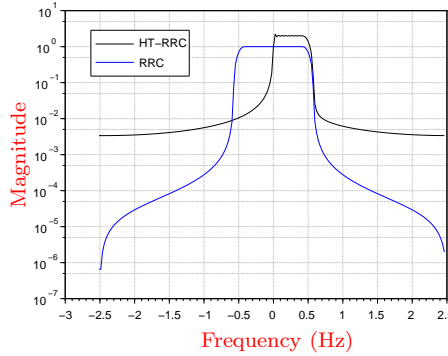


Figure 4: Magnitude response of $p(t)$ and $\tilde{p}(t)$. $|P(0)| = 1$ for RRC, $|\tilde{P}(0)| = 1$ for HT-RRC.

The magnitude response of $p(mT_s)$ (RRC) and $\tilde{p}(mT_s)$ (HT-RRC) given by

$$\tilde{p}(mT_s) = p(mT_s) + j\hat{p}(mT_s) \quad (28)$$

is shown in Figure 4 for $T = 1$ sec, $\rho = 0.161$ and sampling frequency $F_s = 1/T_s = 5$ Hz. Both $p(mT_s)$ and $\hat{p}(mT_s)$ lie in the range $-M \leq m \leq M$ for $M = 100$. The parameter M is referred to as the one-sided window length. Note that in Figure 4, $\tilde{P}(\cdot)$ is the discrete Fourier transform of $\tilde{p}(\cdot)$ given in (28).

The ratio of signal-to-interference (SIR) power is defined as

$$\text{SIR} = 10 \log_{10} \left[\frac{R_{gg}^2(0)}{\sum_{n \neq 0}^n R_{gg}^2(nT)} \right] \text{ db.} \quad (29)$$

where $g(\cdot)$ is $p(\cdot)$ or $\hat{p}(\cdot)$. Note that

$$\begin{aligned} R_{gg}(mT_s) &= g(mT_s) \star g(-mT_s) \\ R_{gg}(nT) &= R_{gg}(nIT_s) \\ I &= \frac{T}{T_s} \end{aligned} \quad (30)$$

where “ \star ” denotes (discrete-time) linear convolution and I is the interpolation factor. The SIR in decibels is shown in Table 1 for different values of the one-sided window length M when $T = 1$ sec, $\rho = 0.161$, $F_s = 5 = 1/T_s$ Hz. We find from Table 1 that the SIR of $R_{\hat{p}\hat{p}}(t)$ is much lower than $R_{pp}(t)$ for the same values of M . This is probably because the signum function in the Hilbert transform (see (19)) has a discontinuity at $F = 0$. In the next section, we discuss the modified Hilbert transform that avoids this discontinuity.

Table 1: SIR of $R_{\hat{p}\hat{p}}(nT)$ and $R_{pp}(nT)$.

M	SIR (db)	
	$R_{\hat{p}\hat{p}}(nT)$	$R_{pp}(nT)$
100	16.931	56.921
80	15.934	49.426
40	12.975	40.602
20	9.363	25.212

MODIFIED HILBERT TRANSFORM

Consider the modified Hilbert transform given by [15]

$$\tilde{H}(F) = \begin{cases} e^{j[\pi(F+aF_1)/(2aF_1)+\pi/2]} & \text{for } |F| \leq aF_1 \\ -j & \text{for } F \geq aF_1 \\ j & \text{for } F \leq -aF_1 \end{cases} \quad (31)$$

for $0 < a \leq 1$, which is plotted in Figure 5. Hence the modified Hilbert transform of $p(t)$

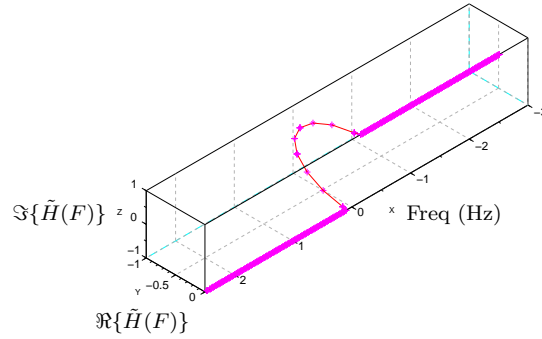


Figure 5: Frequency response of the modified Hilbert transformer for $a = 0.25$, $\rho = 0.161$, $T = 1$ sec.

can be written as

$$\begin{aligned} \hat{p}_m(t) &= \int_{F=-\infty}^{\infty} \tilde{H}(F)P(F)e^{j2\pi Ft} dF \\ &= I_{11} + I_{12} + I_2 \end{aligned} \quad (32)$$

where I_2 is given by (26) and

$$\begin{aligned} I_{11} &= \int_{F=-aF_1}^{aF_1} \tilde{H}(F)P(F)e^{j2\pi Ft} dF \\ &= \frac{-1}{\sqrt{2B}} \int_{F=-aF_1}^{aF_1} e^{j\pi F/(2aF_1)} e^{j2\pi Ft} dF \\ &= \frac{-2aF_1}{\sqrt{2B}} \text{sinc}(aF_1 A_1) \end{aligned} \quad (33)$$

where

$$A_1 = 2t + \frac{1}{2aF_1}$$

$$\text{sinc}(x) = \frac{\sin(\pi x)}{\pi x}. \quad (34)$$

Similarly I_{12} in (32) is equal to

$$\begin{aligned} I_{12} &= \frac{-j}{\sqrt{2B}} \int_{aF_1}^{F_1} e^{j2\pi Ft} dF + \frac{j}{\sqrt{2B}} \int_{-F_1}^{-aF_1} e^{j2\pi Ft} dF \\ &= \frac{2F_1(1+a)}{\sqrt{2B}} \text{sinc}(F_1 t(1+a)) \sin(\pi F_1 t(1-a)). \end{aligned} \quad (35)$$

The magnitude response of $p(mT_s)$ (RRC) and $\tilde{p}_m(mT_s)$ (mHT-RRC) given by

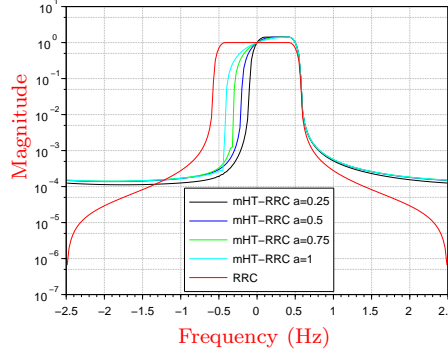


Figure 6: Magnitude response of $p(t)$ and $\tilde{p}_m(t)$. $|P(0)| = 1$ for RRC, $|\tilde{P}_m(0)| = 1$ for HT-RRC.

$$\tilde{p}_m(mT_s) = p(mT_s) + j\hat{p}_m(mT_s) \quad (36)$$

is shown in Figure 6 for $T = 1$ sec, $\rho = 0.161$ and sampling frequency $F_s = 1/T_s = 5$ Hz. Both $p(mT_s)$ and $\hat{p}_m(mT_s)$ lie in the range $-M \leq m \leq M$ for $M = 100$. Note that in Figure 6, $\tilde{P}_m(\cdot)$ is the discrete Fourier transform of $\tilde{p}_m(\cdot)$ given in (36). We find from Table 2

Table 2: SIR of $R_{\hat{p}_m\tilde{p}_m}(nT)$ and $R_{pp}(nT)$.

M	SIR (db)	
	$R_{\hat{p}_m\tilde{p}_m}(nT)$	$R_{pp}(nT)$
100	52.787	56.921
80	45.168	49.426
40	33.298	40.602
20	17.93	25.212

that the SIR of $R_{\hat{p}_m\tilde{p}_m}(nT)$ is comparable to $R_{pp}(nT)$.

DISCRETE TIME SYSTEM MODEL

The discrete time system model used for computer simulations is shown in Figure 7. The input b_k is arranged into frames of length L_{d1} bits and given to the rate-1/2 turbo code [1–3]. The output of the turbo code of length $L_d = 2L_{d1}$ bits is mapped to binary phase shift

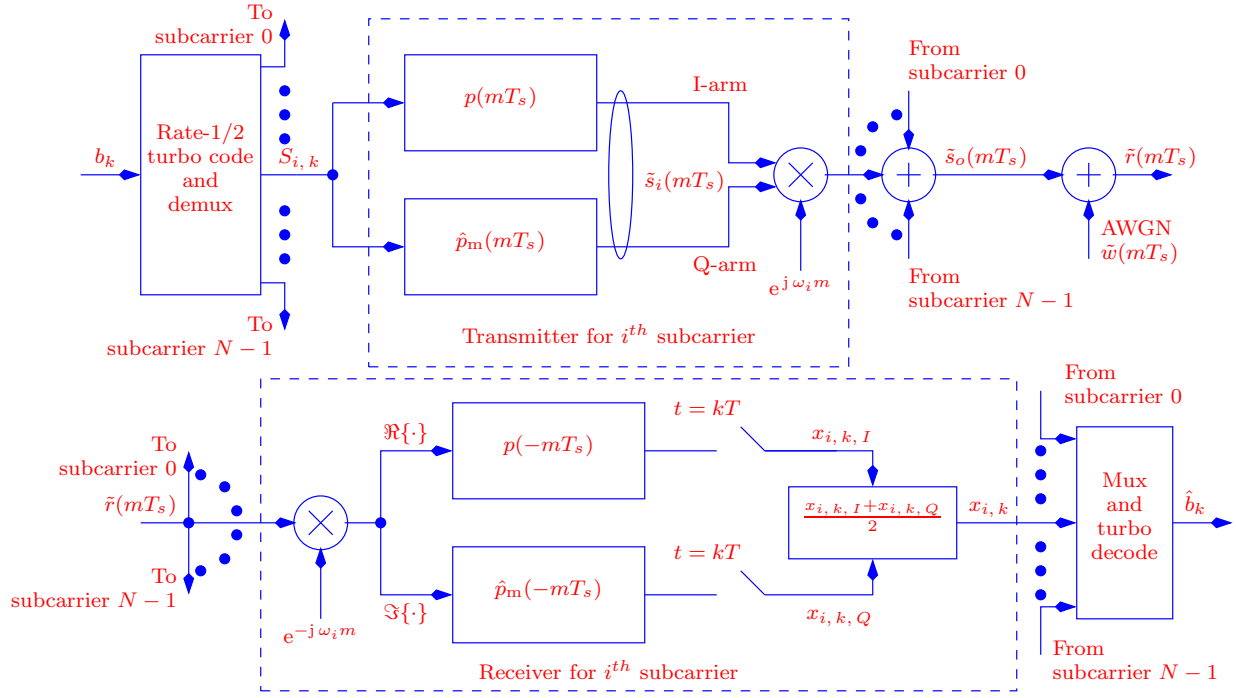


Figure 7: Discrete time system model for OFDM-OQAM.

keyed (BPSK) symbols $S_{i,k} = \pm 1$, demultiplexed and transmitted simultaneously over N subcarriers. The frequency of the i^{th} subcarrier is given by

$$\omega_i = 2\pi i/N \quad \text{radians} \quad \text{for } 0 \leq i \leq N-1 \quad (37)$$

where $N = I$ is the total number of subcarriers and I is given by (30). The overall OFDM-OQAM signal is given by

$$\tilde{s}_o(mT_s) = \sum_{i=0}^{N-1} \tilde{s}_i(mT_s) e^{j\omega_i m} \quad (38)$$

where

$$\tilde{s}_i(mT_s) = \sum_k S_{i,k} \tilde{p}_m(mT_s - kT) \quad (39)$$

where $\tilde{p}_m(\cdot)$ is given by (36). The spectrum of the complex-valued overall OFDM-OQAM

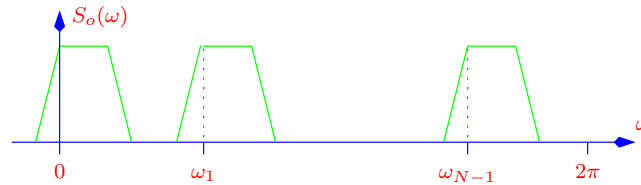


Figure 8: Spectrum of the overall OFDM-OQAM signal $\tilde{s}_o(mT_s)$.

signal $\tilde{s}_o(mT_s)$ is shown in Figure 8, where

$$\omega = 2\pi FT_s \quad \text{radians} \quad (40)$$

where F is the frequency in Hz. Recall that the sampling frequency $1/T_s$ Hz maps to 2π in the digital frequency domain. The variance per dimension of complex-valued additive white

Gaussian noise (AWGN) is

$$\frac{1}{2}E [|\tilde{w}(mT_s)|^2] = \sigma_w^2. \quad (41)$$

The in-phase and quadrature components of $\tilde{w}(mT_s)$ are assumed to be independent. At the receiver we have for the i^{th} subcarrier

$$x_{i,k} = S_{i,k} + z_{i,k} \quad (42)$$

where $z_{i,k}$ denotes real-valued samples of AWGN with variance $\sigma_w^2/2$ [16]. We assume that both $p(\cdot)$ and $\hat{p}_m(\cdot)$ have unit energy, that is

$$\begin{aligned} \sum_{m=-M}^M p^2(mT_s) &= 1 \\ \sum_{m=-M}^M \hat{p}_m^2(mT_s) &= 1. \end{aligned} \quad (43)$$

Note that from (12), (13) and (16), $x_{i,k,I}$, $x_{i,k,Q}$ in Figure 7 have to be summed (or averaged). Since $S_{i,k}$ carries half a bit of information, the average signal-to-noise ratio (SNR) per bit is defined as [16]

$$\begin{aligned} \text{SNR}_{\text{av},b} &= \frac{2E [S_{i,k}^2]}{2\text{D noise variance}} \\ &= \frac{2 \times 1}{2 \times \sigma_w^2/2} \\ &= \frac{2}{\sigma_w^2}. \end{aligned} \quad (44)$$

SIMULATION RESULTS

Table 3: Simulation parameters.

Parameter	Value
$N = I$ (Number of subcarriers = interpolation factor)	256
L_{d1}	1024
L_d	2048
a	0.25
ρ	0.161
M	$8N, 16N$
T	1 sec
T_s	T/N sec

The discrete-time simulation parameters are given in Table 3. The transmit filters are given by $p(mT_s - 0.5T_s)$, $\hat{p}_m(mT_s - 0.5T_s)$, for $-M \leq m \leq M$, for integer m and $M = 8N, 16N$. This is because, we require the filter length to be an integer multiple of N , for the sake of implementation simplicity. The computer simulation results for the bit-error-rate

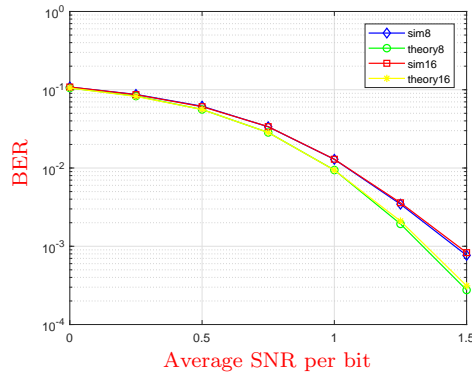


Figure 9: Simulation results.

(BER) vs the average SNR per bit ($\text{SNR}_{\text{av},b}$) are presented in Figure 9. The theoretical BER is obtained from [19]. The BER results for $M = 8N$ are denoted by “sim8” and “theory8”. The BER results for $M = 16N$ are denoted by “sim16” and “theory16”. Observe the close match between theory and simulations.

CONCLUSIONS

This article discusses the implementation of an OFDM-OQAM/FBMC/UFMC system in discrete-time, using Hilbert transform. A simple matched filter receiver is sufficient for detecting the symbols. In the present work, an AWGN channel is considered. Frequency selective fading channels along with carrier frequency offsets can be considered in future works.

References

- [1] K. Vasudevan, “Coherent detection of turbo coded OFDM signals transmitted through frequency selective Rayleigh fading channels,” in *Signal Processing, Computing and Control (ISPCC), 2013 IEEE International Conference on*, Sept. 2013, pp. 1–6.
- [2] —, “Coherent detection of turbo-coded OFDM signals transmitted through frequency selective Rayleigh fading channels with receiver diversity and increased throughput,” *Wireless Personal Communications*, vol. 82, no. 3, pp. 1623–1642, 2015. [Online]. Available: <http://dx.doi.org/10.1007/s11277-015-2303-8>
- [3] —, “Near capacity signaling over fading channels using coherent turbo coded OFDM and massive MIMO,” *International Journal On Advances in Telecommunications*, vol. 10, no. 1 & 2, pp. 22–37, 2017, [Online].
- [4] B. Farhang-Boroujeny, “OFDM versus filter bank multicarrier,” *IEEE Signal Processing Magazine*, vol. 28, no. 3, pp. 92–112, May 2011.
- [5] T. Jiang, C. Ni, D. Qu, and C. Wang, “Energy-efficient NC-OFDM/OQAM-based cognitive radio networks,” *IEEE Communications Magazine*, vol. 52, no. 7, pp. 54–60, 2014.

- [6] C. Kim, Y. H. Yun, K. Kim, and J.-Y. Seol, "Introduction to QAM-FBMC: From waveform optimization to system design," *IEEE Communications Magazine*, vol. 54, no. 11, pp. 66–73, 2016.
- [7] C. Jin, S. Hu, Y. Huang, F. Li, J. Zhang, and S. Ma, "On design of conjugated transmission scheme for FBMC/OQAM systems with interference cancellation," *China Communications*, vol. 14, no. 8, pp. 166–175, 2017.
- [8] F. Yang, Y. Wang, L. Ding, and L. Qian, "An improved equalization with real interference prediction scheme of the FBMC/OQAM system," *China Communications*, vol. 18, no. 1, pp. 120–129, 2021.
- [9] M. T. Gunesser, A. S. Sahab, and C. Seker, "Performance analysis of modulation techniques in 5G communication system," *China Communications*, vol. 19, no. 8, pp. 100–114, 2022.
- [10] Y. Tao, L. Liu, S. Liu, and Z. Zhang, "A survey: Several technologies of non-orthogonal transmission for 5G," *China Communications*, vol. 12, no. 10, pp. 1–15, 2015.
- [11] L. Zhang, A. Ijaz, P. Xiao, and R. Tafazolli, "Multi-service system: An enabler of flexible 5G air interface," *IEEE Communications Magazine*, vol. 55, no. 10, pp. 152–159, 2017.
- [12] Y. Yang and L. Zhu, "Non-orthogonal multi-carrier transmission for internet via satellite," *China Communications*, vol. 14, no. 3, pp. 31–42, 2017.
- [13] A. Nimr, M. Chafii, and G. P. Fettweis, "Unified low complexity radix-2 architectures for time and frequency-domain GFDM modem," *IEEE Circuits and Systems Magazine*, vol. 18, no. 4, pp. 18–31, 2018.
- [14] Y. Yang, L. Zhu, X. Mao, Q. Tan, and Z. He, "The spread spectrum GFDM schemes for integrated satellite-terrestrial communication system," *China Communications*, vol. 16, no. 12, pp. 165–175, 2019.
- [15] K. Vasudevan, G. K. Pathak, S. Kota, and L. Kumar, "OFDM-OQAM using Hilbert transform," 2023, Invited Talk, World Congress on Advanced Materials, 8 - 10 May 2023, Tokyo, Japan. [Online]. Available: <https://www.bitcongress.com/galatechbook3/>
- [16] K. Vasudevan, *Digital Communications and Signal Processing, Second edition (CDROM included)*. Universities Press (India), Hyderabad, www.universitiespress.com, 2010.
- [17] S. Haykin, *Communication Systems*, 2nd ed. Wiley Eastern, 1983.
- [18] K. Vasudevan, *Analog Communications: Problems & Solutions*. Ane Books, Springer, 2018.
- [19] K. Vasudevan, S. Kota, L. Kumar, and H. B. Mishra, "New results on single user massive MIMO," in *MIMO Communications - Fundamental Theory, Propagation Channels, and Antenna Systems*, D. A. Kishk and D. X. Chen, Eds. Rijeka: IntechOpen, 2023, ch. 17. [Online]. Available: <https://doi.org/10.5772/intechopen.112469>